

1 **SEMI-CONSERVATIVE FINITE VOLUME SCHEMES FOR**
2 **CONSERVATION LAWS**

3 ROSA MARIA PIDATELLA*, GABRIELLA PUPPO†, GIOVANNI RUSSO‡, AND PIETRO
4 SANTAGATI§

5 **Abstract.** This paper aims to introduce a new class of high order conservative schemes to solve
6 systems of conservation laws. The idea is to couple the conservation form of the system with, possibly
7 simpler, alternative formulations, which can be used to speed up the time update. In this work, we
8 illustrate the procedure for a Runge Kutta time advancement, but other choices are possible. We
9 show that, as long as the last update is carried out in conservative form, all internal stages can
10 be computed using any consistent non conservative formulation, still ensuring the propagation of
11 shock waves with the correct speeds. The same procedure can be easily extended to finite difference
12 schemes. Tests from classical and relativistic gas dynamics are carried out to study convergence,
13 numerical robustness and performance.

14 **Key words.** high order schemes, hyperbolic systems, method of lines, non conservative variables,
15 relativistic gas dynamics

16 **1. Introduction.** Several physical systems concerning propagation phenomena
17 are modeled by quasilinear hyperbolic systems of conservation laws. Such systems
18 have been widely studied, both for the enormous relevance in the applications and for
19 the mathematical challenges they lead to. As known, even if smooth initial conditions
20 are imposed, the solution of a quasilinear hyperbolic system will in general develop
21 singularities in finite times. After such a time, classical solutions cease to exist, and
22 one has to deal with weak solutions which, for smooth initial data, are composed by
23 piecewise smooth regions separated by jump discontinuities satisfying suitable jump
24 conditions. In general, uniqueness of the weak solution is not guaranteed. It can be
25 restored by adopting some regularization technique, the most common one being the
26 addition of a parabolic term with a small viscosity which produces a unique solution
27 with sharp gradients that become jump discontinuities in the limit as the viscosity
28 parameter vanishes, yielding the so called *viscosity solution*.

29 The mathematical theory of quasilinear systems of conservation laws is a very
30 active field of research, and existence and uniqueness of the solution for several classes
31 of systems have been proven [8].

32 The most common schemes to produce numerical solutions of quasilinear hyper-
33 bolic systems of conservation laws are the so called *shock-capturing schemes*: for-
34 mation and propagation of shocks is automatically “captured” by the scheme, that
35 produces a small region with sharp gradients where the shock forms and propagates.

36 The construction and analysis of shock-capturing schemes has been a very active
37 field of research in recent decades. Such schemes, based on Eulerian approach, are
38 designed to discretize the system on a fixed grid, by finite volume, finite difference or
39 finite element methods.

40 In this paper we will make for the finite volume and finite difference schemes,
41 which, together with discontinuous Galerkin schemes, are the most commonly used
42 methods in this context. An account of finite volume schemes for conservation laws
43 can be found in the book by Le Veque [18], whereas a more mathematical oriented

*Università degli Studi di Catania, Catania, Italy(rosa@dmi.unict.it)

†La Sapienza Università di Roma, Roma, Italy(gabriella.puppo@uniroma1.it)

‡Università degli Studi di Catania, Catania, Italy(russo@dmi.unict.it)

§Tass International, a Siemens Business(pietro.santagati@tassinternational.com)

44 book is the one by Godlewski and Raviart [11].

45 In finite volume schemes, the conservation laws are integrated in space over each
46 grid cell of the domain, obtaining in such a way evolution equations for the cell
47 averages of variables. The unknowns are now the cell average values, which are
48 modified in each time step by the flux through the edges of each cell, and then the
49 choice of the proper numerical flux functions which correctly approximate the flux is a
50 crucial point of the scheme. This flux can be obtained by the computation of numerical
51 flux functions, for example Godunov, Engquist-Osher, Rusanov, at the edge of each
52 cell, extracting information on point values from the knowledge of the cell averages.
53 This is obtained through an appropriate non linear reconstruction algorithm, such as
54 ENO or WENO [31], or the more recent CWENO, [6]. In this way we get, from the
55 original system of PDE's, a large system of ODE's for the cell averages. This procedure
56 is called method of lines, and it yields a semidiscrete system. Once a system of ODE's
57 is derived, suitable integrators, such as Strongly Stability Preserving (SSP) Runge-
58 Kutta can be used [12], providing high order accuracy in time, without any spurious
59 oscillations due to time discretization. A conservative discrete form is mandatory in
60 those regions containing discontinuities, because otherwise their speed propagation
61 might be computed inexactly.

62 In the above approach, and in most finite volume schemes, the basic unknowns
63 are the conservative variables and the equations are always treated in conservative
64 form. However, in many cases there are more convenient ways to write the system
65 of equations. Harabetian and Pego [14] proposed a hybrid approach, whereby the
66 system is solved by a non conservative scheme in smooth regions, and switches to a
67 conservative form in regions with discontinuities. This approach allowed considerable
68 savings in computational time.

69 An alternative to the semidiscrete finite volume schemes described before is offered
70 by central schemes on staggered grids. After the first second order shock capturing
71 central scheme on staggered grid in one space dimension by Nessyahu and Tadmor [24],
72 several extensions appeared, increasing the order of accuracy [2, 19], and the spatial
73 dimensions [16] or both [21].

74 In such schemes, a piecewise smooth solution is reconstructed in each cell starting
75 from the cell averages at a given time level t^n . At variance with semidiscrete schemes,
76 in central schemes the fluxes are evaluated at the cell center, along time, enjoying
77 the smoothness of the solution for short times, provided a suitable restriction of CFL
78 type on the time step is satisfied. An advantage that has been attributed to central
79 schemes lies in their construction. They do not require to use exact or approximate
80 Riemann solvers, which are needed for schemes based on the solution of Riemann
81 problems. Such advantage, however, is not the main feature. Actually, the choice of
82 the numerical flux function implies a choice of a particular Riemann solver: a great
83 flexibility of such functions is available, ranging from the Godunov flux, based on the
84 exact solution of the Riemann problem, to the Rusanov flux (also called local Lax-
85 Friedrichs), which only needs an estimation of the Jacobian's spectral radius of the
86 system. Staggered central schemes do not have this choice, and are less effective. For
87 instance, the treatment of contact discontinuities in gas dynamics, that are smeared
88 much more than in the case of sharper Riemann solvers. In practice, the choice of the
89 numerical flux function is actually a *weakness* of staggered central schemes, and not
90 an advantage!

91 There is, however, a great advantage of high order staggered central schemes over
92 classical non staggered schemes. Since the fluxes are evaluated from a preliminary
93 computation of the solution at the center of each cell, where the solution is (locally)

94 smooth, a large flexibility is provided in the evaluation of such preliminary solution.
 95 This feature was already pointed out by Nessyahu and Tadmor in their original paper,
 96 where they noticed that the so called *predictor value*, at cell center and half time step,
 97 could be computed by the equation written in conservative form (discretizing the flux)
 98 or in non conservative form (written using the product of the Jacobian matrix times
 99 the space derivative of the solution).

100 That feature was further exploited in [25]. In such a paper, a method was pre-
 101 sented, whereby the numerical solution on a staggered grid is computed by a conser-
 102 vative scheme. In this scheme the stage values, needed for the computation of the
 103 fluxes at the Runge-Kutta stages, may be computed by discretizing the equation in
 104 non conservative form. This procedure allows to get a large flexibility in choosing the
 105 dependent variables. However, in spite of this large flexibility, Central Runge-Kutta
 106 (CRK) methods suffered the lack of flexibility in choosing the numerical flux function,
 107 typical of staggered central schemes. Furthermore, the formulation of the boundary
 108 conditions might be a little bit more complicated.

109 In the present paper we propose a new class of schemes, which enjoy the flex-
 110 ibility of CRK in the choice of the possibly non conservative form of the equation
 111 to be discretized in time, while, at the same time, permitting the usage of arbitrary
 112 numerical flux functions at the cell edges, thus delivering sharp treatment of contacts
 113 and linear discontinuities. The stage values are computed at the cell center, where
 114 the solution is locally smooth, by writing the system in a not necessarily conservative
 115 form. Once the (non conservative) stage values are computed, a preliminary solu-
 116 tion is reconstructed at both cell edges, by some suitable non oscillatory technique.
 117 The reconstructed values are used to compute the fluxes at the cell edges, by some
 118 numerical flux function. Once the fluxes are known, the cell averages are updated
 119 by the conservative Runge-Kutta step for the computation of the numerical solution.
 120 Therefore, the final scheme is in conservative form, though most calculations can be
 121 performed using a convenient non conservative form of the equation.

122 The larger flexibility of the new approach allows the construction of more efficient
 123 schemes, in all those cases in which the system has a simpler form when expressed
 124 in non conservative variables. A typical example is given by the Euler equations of
 125 relativistic gas dynamics, in which the computation of the pressure by the conservative
 126 variables requires the solution of a non linear equation. The new approach allows
 127 to compute pressure just once per time step in each cell, as opposed to s times
 128 for a classical s -stage Runge-Kutta scheme applied to a semidiscrete finite volume
 129 discretization.

130 The plan of the paper is the following. In the next section we describe the
 131 construction of finite volume schemes based on non conservative evolution of the fields
 132 at the cell center, in one spatial dimension. Then we present a series of numerical
 133 tests both for classical gasdynamics and for the relativistic case. The purpose of the
 134 tests is to asses the high resolution capability and the computational efficiency of the
 135 new approach. Finally in the last section we draw conclusions and mention future
 136 perspectives of the new approach.

137 **2. Semi-conservative finite volume schemes.** The evolution of conserved
 138 quantities, such as mass, momentum and energy, is given by equations of the form

139 (2.1)
$$\partial_t \int_V u \, dv + \int_{\partial V} f(u) \cdot n \, dS = 0, \quad \forall V \in \mathbb{R}^d,$$

140 where $u : \mathbb{R}^d \times \mathbb{R}^+ \rightarrow \Omega \subset \mathbb{R}^m$ are the conserved quantities, $f = [f_1, \dots, f_d] : \mathbb{R}^m \rightarrow$
141 \mathbb{R}^m is the flux function, and V is any control volume in \mathbb{R}^d . Here Ω denotes the
142 set where the variable u is defined: for instance, the density must be positive. If u
143 is smooth, (2.1) can be rewritten as a system of partial differential equations of the
144 form

$$145 \quad (2.2) \quad u_t + \nabla \cdot f = 0.$$

146 It is well known that the solution u can develop singularities in a finite time, even
147 from smooth initial data. In this case, (2.2) must be interpreted in a weak sense,
148 while (2.1) continues to hold, see [8] for more details.

149 Piecewise smooth solutions of eq. (2.1) are allowed, in which jump discontinuities
150 propagate satisfying the co-called Rankine-Hugoniot conditions, which are derived
151 from (2.1). Since (2.2) descends from the conservative principle (2.1), the equations
152 (2.2) are called in *conservative form*. They are the only equations consistent with
153 (2.1) which permit to derive the correct Rankine Hugoniot conditions, and thus the
154 correct shock speeds.

155 Here, for simplicity, we consider initial value problems for one dimensional, quasi-
156 linear hyperbolic systems of conservation laws of the form

$$157 \quad (2.3) \quad \begin{cases} u_t + f_x(u) &= 0 & t > 0 \\ u(x, 0) &= u_0(x). & x \in \mathbb{R} \end{cases}$$

158 Since the system is hyperbolic, the Jacobian $A(u) = \nabla_u f$ is diagonalizable with
159 real eigenvalues. As long as the solution is differentiable, system (2.3) can be rewritten
160 in the non conservative form

$$161 \quad (2.4) \quad u_t + A(u)u_x = 0,$$

162 completed by the same initial conditions. For generic quasilinear systems, the Jaco-
163 bian matrix A depends explicitly on the solution u .

164 The key point of this work is that other non conservative forms of system (2.3) can
165 be formulated, as long as the solution is smooth, which can be more convenient from
166 a computational point of view, and it is possible to exploit these simpler formulations,
167 without loosing exact conservation at the discrete level.

168 Let v denote a new set of variables, related to u by a one to one smooth mapping
169 $\mathcal{M}(v)$:

$$170 \quad (2.5) \quad u = \mathcal{M}(v), \quad J = \frac{\partial \mathcal{M}}{\partial v}, \quad \mathbf{det}(J) \neq 0, \quad \forall v \in \mathcal{M}^{-1}(\Omega).$$

171 Rewriting system (2.3) in terms of the new set of variables, we get

$$172 \quad (2.6) \quad \begin{cases} v_t + B(v)v_x &= 0 & t > 0 \\ v(x, 0) &= v_0(x) = \mathcal{M}^{-1}(u_0(x)) & x \in \mathbb{R} \end{cases}$$

173 where $v : \mathbb{R} \times \mathbb{R}^+ \rightarrow \mathcal{M}^{-1}(\Omega) \subset \mathbb{R}^m$, $B = J^{-1}AJ$.

174 We will solve (2.3) with the method of lines. To this end, we cover the compu-
175 tational domain with cells centered on the points $x_j \in \mathbb{R}, j \in \mathbb{Z}$. For simplicity, we
176 consider a uniform grid, such that $x_{j+1} - x_j \equiv \Delta x, \forall j$. Let $I_j = [x_{j-1/2}, x_{j+1/2}]$ be
177 the generic cell, enclosed by the interfaces $x_{j-1/2} = x_j - \frac{\Delta x}{2}$, $x_{j+1/2} = x_j + \frac{\Delta x}{2}$.

178 Let us introduce the cell averages

$$179 \quad (2.7) \quad \bar{u}_j(t) = \frac{1}{\Delta x} \int_{x_{j-1/2}}^{x_{j+1/2}} u(x, t) dx, \quad j \in \mathbb{Z}.$$

180 Integrating system (2.3) over the cells I_j , one obtains the finite volume formulation

$$181 \quad (2.8) \quad \frac{d\bar{u}_j}{dt} = -\frac{1}{\Delta x} (f(u(x_{j+1/2}, t)) - f(u(x_{j-1/2}, t))),$$

$$182 \quad \bar{u}_j(0) = \frac{1}{\Delta x} \int_{x_{j-1/2}}^{x_{j+1/2}} u_0(x) dx, \quad j \in \mathbb{Z}.$$

183 The numerical solution of system (2.3) in finite volume form (2.8) is based on three
184 key points

- 185 1. a reconstruction algorithm \mathcal{R} , which gives an estimate of the numerical solu-
186 tion at the interfaces, starting from the cell averages, with the desired accu-
187 racy;
- 188 2. a numerical flux function $F_{j+1/2}$, approximating $f(u(x_{j+1/2}, t))$ at each cell
189 interface;
- 190 3. a time advancing scheme to compute the solution at time $t^n + \Delta t$, starting
191 from time t^n .

192 The purpose of the reconstruction algorithm \mathcal{R} is to obtain estimates of the point
193 values of the solution at the cell interfaces, starting from the cell averages. Typically,
194 one works with piecewise polynomial reconstructions,

$$195 \quad \mathcal{R}(x, \bar{\mathbf{u}}) = \sum_j P_j(x) \chi_{I_j}(x),$$

196 where $P_j(x)$ are polynomials of degree d , which match $d+1$ contiguous cell averages,
197 including \bar{u}_j , and where $\bar{\mathbf{u}}$ denotes the vector containing all cell averages of the numer-
198 ical solution. Note that the reconstruction is discontinuous across cells. In particular,
199 let

$$200 \quad u_{j+1/2}^+ = P_{j+1}(x_{j+1/2}) \quad u_{j+1/2}^- = P_j(x_{j+1/2})$$

201 be the *boundary extrapolated data* at the cell interfaces. If the solution is smooth, and
202 the data are reconstructed with accuracy p , then the jump at the interface $u_{j+1/2}^+ -$
203 $u_{j+1/2}^- = O(\Delta x)^p$.

204 The numerical flux $F_{j+1/2}$ is a function of the two estimates of the solution at
205 the interface, namely $F_{j+1/2} = F(u_{j+1/2}^+, u_{j+1/2}^-)$ and it is a numerical approximation
206 of the flux $f(u)$ at the cell interface, obtained solving numerically (or exactly) the
207 Riemann problem at the interface defined by the data $u_{j+1/2}^+$ and $u_{j+1/2}^-$. Many
208 popular numerical fluxes can be written in viscous form as

$$209 \quad (2.9) \quad F(u^+, u^-) = \frac{1}{2} (f(u^+) + f(u^-)) - \frac{1}{2} Q(u^+, u^-) (u^+ - u^-),$$

210 where $Q(u^+, u^-)$ is the viscosity matrix. For instance, for local Lax-Friedrichs (called
211 also Rusanov flux) one has

$$212 \quad Q(u^+, u^-) = \alpha(u^+, u^-) \mathbb{I},$$

213 where, if f is convex, $\alpha = \max(\rho(A(u^+), \rho(A(u^-))) = \max(\rho(B(v^+), \rho(B(v^-)))$.
 214 Other choices lead to less dissipative numerical monotone fluxes¹. For example, if
 215 a Roe matrix $A(u^+, u^-)$ [28] is available one could use

$$216 \quad Q(u^+, u^-) = |A(u^+, u^-)|$$

217 or some approximation of the absolute value of the matrix which is cheaper to compute
 218 and does not require full characteristic decomposition of the matrix. Approaches based
 219 on the approximation of the matrix absolute value have been introduced in [9], and
 220 has been then generalized in various contexts (see, for example, the recent paper [5]).

221 The reconstruction \mathcal{R} and the numerical flux F provide the space discretization
 222 of the scheme. With these ingredients, the semidiscrete form of system (2.8) is given
 223 by the system of ODE's

$$224 \quad (2.10) \quad \frac{d\bar{u}_j}{dt} = -\frac{1}{\Delta x} \left[F(u_{j+1/2}^+(t), u_{j+1/2}^-(t)) - F(u_{j-1/2}^+(t), u_{j-1/2}^-(t)) \right], \quad j \in \mathbb{Z}.$$

225 Any numerical method for the integration of systems of ODE's can be used as
 226 time advancing scheme to solve (2.10). In this work, we will use explicit Runge-Kutta
 227 methods, [13]. For a generic initial value problem (IVP) of the form

$$228 \quad \begin{aligned} \frac{dy}{dt} &= g(t, y(t)), & y(t) : \mathbb{R} &\rightarrow \mathbb{R}^d, & d \in \mathbb{N}, \\ y(t_0) &= y_0 \end{aligned}$$

229 an explicit ν -stage Runge Kutta scheme can be written as

$$230 \quad (2.11) \quad y^{n+1} = y^n + \Delta t \sum_{l=1}^{\nu} b_l g(t^n + c_l \Delta t, Y^{(l)}), \quad (\text{corrector step})$$

$$231 \quad (2.12) \quad Y^{(l)} = y^n + \Delta t \sum_{k=1}^{l-1} a_{lk} g(t^n + c_k \Delta t, Y^{(k)}), \quad (\text{predictor step})$$

$$232 \quad l = 1, \dots, \nu$$

233 where $\{Y^{(l)}\}_{l=1, \dots, \nu}$ are the internal stages of the Runge Kutta step (also known as
 234 *stage values*).

235 The coefficients $\{c_l\}_{l=1, \dots, \nu}$, $\{b_l\}_{l=1, \dots, \nu}$, $\{a_{ij}\}_{i,j=1, \dots, \nu}$ univocally identify the
 236 numerical scheme. In standad finite volume (FV) schemes with Runge Kutta time
 237 advancement, the evolution of the numerical solution (2.11) is obtained applying the
 238 Runge-Kutta scheme to the semidiscrete form (2.10):

$$239 \quad (2.13) \quad \begin{aligned} \bar{u}_j^{n+1} &= \bar{u}_j^n - \frac{\Delta t}{\Delta x} \sum_{l=1}^{\nu} b_l \Delta F_j^{(l)}, \\ \bar{u}_j^{(l)} &= \bar{u}_j^n - \frac{\Delta t}{\Delta x} \sum_{k=1}^{l-1} a_{lk} \Delta F_j^{(k)}, \quad l = 1, \dots, \nu, \\ \Delta F_j^{(l)} &= F(u_{j+1/2}^{(l)+}, u_{j+1/2}^{(l)-}) - F(u_{j-1/2}^{(l)+}, u_{j-1/2}^{(l)-}), \end{aligned}$$

242 where the values $u_{j+1/2}^{(l)\pm}$, at each cell interface are computed with a reconstruction step
 243 from the cell averages $\bar{u}^{(l)}$. Thus, the conservative form of the equation is used for the

¹A numerical flux $F(u^+, u^-)$ is said to be monotone if the first order scheme produced by the flux is a monotone scheme, i.e. if $u_j^n \geq w_j^n \forall j$, then $u_j^{n+1} \geq w_j^{n+1} \forall j$. For more details consult [17].

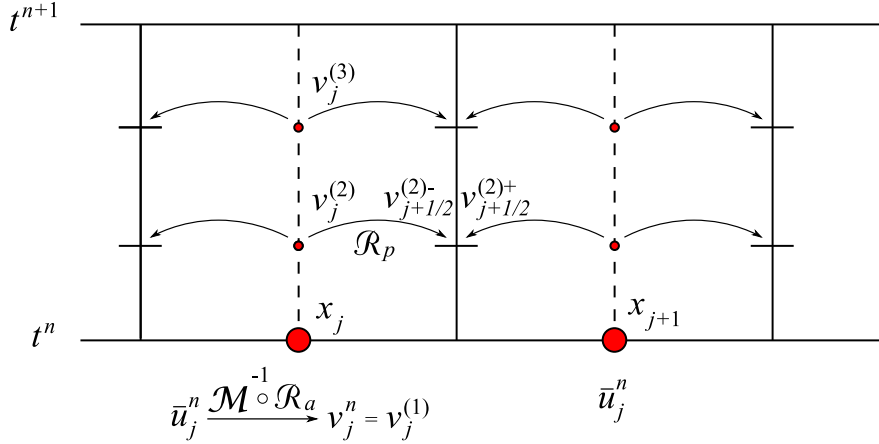


FIG. 2.1. Diagram for semi-conservative finite-volume schemes. At time t^n the cell averages are known. Pointwise values u_j^n are computed at cell centers, and then converted to the non-conservative variables v_j^n . Such variables are evolved in time and the corresponding stage values $v_j^{(k)}$ are computed at position x_j and time $t^n + c_k \Delta t$. The stage values are reconstructed at each cell edge, obtaining $v_{j \pm 1/2}^{(k)}$. From such values the numerical flux at the quadrature nodes in time is computed, and adopted in order to obtain the conservative approximation of cell average at the new time t^{n+1} .

244 final update (corrector step), and also for each of the ν stage values. This is precisely
 245 the point where our new SC (semiconservative) schemes differ from traditional finite
 246 volume FC (fully conservative) schemes.

247 In the semiconservative SC approach we propose, we first seek for an alternative
 248 simple formulation of the equations in the form (2.6), for a new set of variables v ,
 249 defined by the smooth one to one mapping (2.5). We then use the conservative form
 250 of the equation for the final update, but each of the stage values is computed using
 251 the simpler system $v_t + B(v)v_x = 0$. Clearly, the convenience of the method depends
 252 on how much simpler system (2.6) is with respect to the conservative formulation,
 253 and on the number of stages ν . Thus, this approach is particularly interesting for
 254 high order schemes.

255 More precisely, from the initial cell averages \bar{u}^n , we apply a reconstruction step
 256 which yields the point values u_j^n at the cell centers. From these, we compute $v_j^n =$
 257 $\mathcal{M}^{-1}(u_j^n)$, $\forall j$. Next, the stages are computed from (2.6) as

$$258 \quad (2.14) \quad v_j^{(l)} = v_j^n - \Delta t \sum_{k=1}^{l-1} a_{lk} B(v_j^{(k)}) (D_x v^{(k)})_j, \quad l = 1, \dots, \nu.$$

259 Here $(D_x v^{(k)})_j$ denotes the numerical discretization of the space derivative of the data
 260 $v^{(k)}$, obtained with a suitable reconstruction. After all stages have been computed
 261 using the simple system (2.14), the boundary extrapolated data at the l -th stage are
 262 obtained with a reconstruction step on the point values $v_j^{(l)}$, and the conservative
 263 variables u are recovered from $u_{j+1/2}^{(l)+} = \mathcal{M}(v_{j+1/2}^{(l)+})$ and $u_{j+1/2}^{(l)-} = \mathcal{M}(v_{j+1/2}^{(l)-})$. These
 264 quantities are used to close the time step with equation (2.13).

265 The algorithm is illustrated in Fig. 2.1 and in the box appearing in Fig. 2.2. Note
 266 that different reconstructions are needed: \mathcal{R}_a is the reconstruction which computes

Algorithm: SC schemes

- From $\bar{\mathbf{u}}^n$ find the pointvalues $u_j^n = \mathcal{R}_a(x_j, \bar{\mathbf{u}}^n)$, $\forall j$.
- Compute $v_j^n = \mathcal{M}^{-1}(u_j^n)$, $\forall j$.
- Compute all stage values $v_j^{(l)}$ from eq. (2.14) $\forall j$.
- Compute the values at interfaces $v_{j+1/2}^{(l)\pm} = \mathcal{R}_p(x_{j+1/2}, \mathbf{v}^{(l)})$, $\forall j$.
- Go back to conservative variables $u_{j+1/2}^{(l)\pm} = \mathcal{M}(v_{j+1/2}^{(l)\pm})$, $\forall j$.
- Close the time step on conservative variables with equation (2.13).

FIG. 2.2. Algorithm for the semi-conservative finite-volume schemes

267 point values from cell averages, while \mathcal{R}_p yields boundary extrapolated data from
 268 point values, and D_x is a discrete derivative.

269 **2.1. Constructing high order SC schemes.** Semiconservative schemes can
 270 be constructed with any order of accuracy. To obtain a scheme of order p , the re-
 271 constructions and the time advancement Runge-Kutta scheme must be of matching
 272 order. Here we will consider second, third and fourth order schemes.

273 **Second order.** Since, for a smooth function $w(x)$, $w(x_j) = \bar{w}_j + O(\Delta x)^2$, at
 274 second order accuracy the reconstruction \mathcal{R}_a is the identity. From the point values
 275 \mathbf{w} , the approximate slopes σ_j are computed with a piecewise linear reconstruction
 276 and a limiter such as MinMod, see [17] and references therein. Thus, $\forall j$ we have:

$$\begin{aligned}
 277 \quad & u_j^n = \bar{u}_j^n, \\
 278 \quad & v_j^n = \mathcal{M}(u_j^n) \\
 279 \quad & \sigma_j = D_x v|_j \\
 280 \quad & v_{j+1/2}^+ = v_{j+1}^n - \frac{1}{2}\Delta x \sigma_{j+1}, \quad v_{j+1/2}^- = v_j^n + \frac{1}{2}\Delta x \sigma_j \\
 281 \quad &
 \end{aligned}$$

282 where the slopes σ are computed from the data \mathbf{v} . Then the scheme proceeds as in
 283 Fig. 2.2. Note that the same reconstruction is used to compute the point values, the
 284 discrete derivative $\sigma = D_x v$ in (2.14) and the boundary extrapolated data.

285 The SSP second order Heun scheme is used for the time advancement.

286 **Fourth order.** All reconstructions are obtained with WENO type interpolations,
 287 see [32], [3] and the review [31]. For a fourth order scheme, the reconstruction is based
 288 on three parabolas, combined in order to maximize accuracy on smooth solutions, but,
 289 at the same time, preventing spurious oscillations on non smooth data. The generic
 290 WENO reconstruction can be written as

$$291 \quad \mathcal{R}(x, \bar{\mathbf{u}}) = \sum_{\ell=-1}^1 \omega_j^\ell P_{j+\ell}(x).$$

292 When reconstructing point values from cell averages (\mathcal{R}_a), the parabolas $P_{j+\ell}$ inter-
 293 polate the data $\bar{u}_{j+\ell}$ in the sense of averages:

$$294 \quad \frac{1}{\Delta x} \int_{I_{j+\ell}} P_j(x) = \bar{u}_{j+\ell}, \quad \ell = -1, 0, 1,$$

295 while the reconstruction from point values \mathcal{R}_p has $P_j(x_{j+l}) = u_{j+l}, l = -1, 0, 1$. In
 296 both cases, the generic parabola $P_j(x) = P(x; w_{j-1}, w_j, w_{j+1})$ is given by
 (2.15)

$$297 \quad P_j(x) = w_j - \frac{C}{24}(w_{j+1} - 2w_j + w_{j-1}) + \frac{w_{j+1} - w_{j-1}}{2\Delta x}(x - x_j) + \frac{w_{j+1} - 2w_j + w_{j-1}}{2\Delta x^2}(x - x_j)^2,$$

298 with $C = 1, w_\ell = \bar{u}_\ell, \ell = j - 1, j, j + 1$ for \mathcal{R}_a and $C = 0, w_\ell = u_\ell, \ell = j - 1, j, j + 1$
 299 for \mathcal{R}_p . The nonlinear weights $\{\omega_j^\ell\}$ are

$$300 \quad (2.16) \quad \omega_j^\ell = \frac{\alpha_j^\ell}{\sum_{k=-1}^1 \alpha_j^k}, \quad \alpha_j^\ell = \frac{d^\ell}{(\varepsilon + \beta_j^\ell)^2}, \quad \ell = -1, 0, 1.$$

301 The smoothness indicators β_j^ℓ prevent the selection of stencils with non smooth data,
 302 thus controlling spurious oscillations. In the case of parabolas they are given by, see
 303 [31],

$$304 \quad \beta_j^{-1} = \frac{13}{12}(\bar{u}_{j-2} - 2\bar{u}_{j-1} + \bar{u}_j)^2 + \frac{1}{4}(\bar{u}_{j-2} - 4\bar{u}_{j-1} + 3\bar{u}_j)^2,$$

$$305 \quad \beta_j^0 = \frac{13}{12}(\bar{u}_{j-1} - 2\bar{u}_j + \bar{u}_{j+1})^2 + \frac{1}{4}(\bar{u}_{j-1} - \bar{u}_{j+1})^2,$$

$$306 \quad \beta_j^1 = \frac{13}{12}(\bar{u}_j - 2\bar{u}_{j+1} + \bar{u}_{j+2})^2 + \frac{1}{4}(3\bar{u}_j - 4\bar{u}_{j+1} + \bar{u}_{j+2})^2.$$

307 The parameter ε prevents division by zero, but it is also involved in the accuracy of
 308 the scheme, see [1] or [7]. Here we choose simply $\varepsilon = 10^{-6}$, as in [31].

309 A key point is the choice of the constants d_ℓ . When the data derive from a smooth
 310 function, all smoothness indicators are approximately equal, and the weights $\omega_j^\ell \simeq d^\ell$.
 311 Then the constants d_ℓ are determined maximizing the accuracy that can be obtained
 312 with a convex combination of the three parabolas involved. The problem is that a
 313 convex combination of three parabolas can provide uniform accuracy within the cell
 314 only up to third order, even though the stencil contains 5 cells. To increase accuracy,
 315 the constants are determined maximizing the accuracy of the reconstruction at one
 316 particular point. Note that each quantity being reconstructed needs a specific set of
 317 constants, and thus a different reconstruction.

318 A fourth order reconstruction of point values from cell centers can be obtained
 319 by any symmetric choice of the constants $d_\ell, \ell = -1, 0, 1$, as illustrated in [19]. We
 320 use $d^{-1} = 3/16, d^0 = 5/8, d^1 = 3/16$. Higher order accuracy is possible (indeed
 321 sixth order can be obtained), however it requires the use of negative weights. This
 322 problem can be tackled with the technique described in [30], but we will not consider
 323 this case here. For reconstructing the boundary extrapolated data, the constants are
 324 $d^{-1} = 5/16, d^0 = 5/8, d^1 = 1/16$ for the left value $v_{j-1/2}^+$, and $d^{-1} = 1/16, d^0 =$
 325 $5/8, d^1 = 5/16$ for the right value $v_{j+1/2}^-$. The accuracy of the reconstructed data is
 326 5, for smooth functions.

327 Finally, a reconstruction is needed also to compute the numerical derivative D_x .
 328 Now, the reconstruction is given by

$$329 \quad D_x v|_{x_j} = \mathcal{R}_D(x_j, \mathbf{v}) = \sum_{\ell=-1}^1 \omega_j^\ell \frac{d}{dx} P_{j+\ell}(x_j).$$

330 The accuracy constants in this case are $d^{-1} = 1/6, d^0 = 2/3, d^1 = 1/6$, and the
 331 accuracy of $D_x v|_{x_j}$ is 4.

332 A class of WENO type reconstructions with uniform accuracy within the whole
 333 cell can be found in [6]: in this case a single reconstruction step can yield all needed
 334 quantities. We will illustrate this technique for constructing a third order scheme in
 335 the next paragraph.

336 The time advancement scheme is the standard fourth order Runge-Kutta scheme.
 337 In all cases, the numerical flux used is the Lax-Friedrichs flux.

338 **Third order.** The reconstruction used here is taken from [20], and can be viewed
 339 as a particular case of [6], leading to a third order scheme.

340 Consider a set of data (point values or cell averages) and a polynomial P_{opt} of
 341 degree G , which interpolates in some sense all the given data (*optimal polynomial*).
 342 The CWENO operator computes a reconstruction polynomial

$$343 \quad P_{\text{rec}} = \text{CWENO}(P_{\text{opt}}, P_1, \dots, P_m) \in \mathbb{P}^G$$

344 using $P_{\text{opt}} \in \mathbb{P}^G$ and a set of lower order alternative polynomials $P_1, \dots, P_m \in \mathbb{P}^g$,
 345 where $g < G$ and $m \geq 1$. The definition of P_{rec} depends on the choice of a set of
 346 positive real coefficients $d_0, \dots, d_m \in [0, 1]$ such that $\sum_{\ell=0}^m d_\ell = 1$, $d_0 \neq 0$ (called
 347 *linear coefficients*) as follows:

348 1. first, introduce the polynomial P_0 defined as

$$349 \quad (2.17) \quad P_0(x) = \frac{1}{d_0} \left(P_{\text{opt}}(x) - \sum_{\ell=1}^m d_\ell P_\ell(x) \right) \in \mathbb{P}^G$$

350 2. then the nonlinear coefficients ω_ℓ are computed from the linear ones as in
 351 (2.16) where β_ℓ denotes suitable regularity indicators, which can be chosen
 352 following [15] as

$$353 \quad (2.18) \quad \beta_\ell = \sum_{k \geq 1} \Delta x^{2k-1} \int_{x_j-1/2}^{x_j+1/2} \left(\frac{d^k}{dx^k} P_\ell(x) \right)^2 \Delta x, \quad \ell = 0, \dots, m$$

354 3. and finally

$$355 \quad (2.19) \quad P_{\text{rec}}(x) = \sum_{\ell=0}^m \omega_\ell P_\ell(x) \in \mathbb{P}^G.$$

356 In the case of a third order scheme, the degree of P_{opt} and P_0 is $G = 2$, while the
 357 $m = 2$ lower degree polynomials are just linear functions. The interesting point is that
 358 since P_{rec} is defined everywhere in the cell one can use it to compute the extrapolated
 359 data and the discrete derivative. The constants d^ℓ can be chosen quite freely. Here
 360 we have $d_0 = \frac{1}{2}$, $d_1 = d_2 = \frac{1}{4}$.

361 As time integrator, we employ the third order Runge Kutta scheme used in [15].

362 **3. SC schemes and Lax Wendroff's Theorem.** A crucial issue in the in-
 363 tegration of systems of conservation laws is the enforcement of exact conservation.
 364 If shock waves appear, exact conservation ensures that the correct wave speeds are
 365 captured also at the numerical level. This result is guaranteed by Lax Wendroff's The-
 366 orem which contains sufficient conditions for the convergence of a numerical scheme
 367 to a weak solution of conservation laws.

368 The key fact is that Lax Wendroff's Theorem (see for instance [10, pag. 100]) re-
 369 quires the scheme to be *conservative*, and this is the main reason why one discretizes

370 directly the conservative form of the equations, thus working in conservative vari-
 371 ables. However, recalling the definition of conservative scheme, we can easily prove
 372 that SC schemes are indeed conservative, and therefore satisfy the hypotheses of Lax
 373 Wendroff's Theorem.

374 **DEFINITION 3.1. Conservative scheme** *The numerical scheme*

375
$$\bar{u}_j^{n+1} = \bar{u}_j^n - \frac{\Delta t}{\Delta x} (F_{j+1/2} - F_{j-1/2})$$

376 *is conservative if the numerical flux $F_{j+1/2} = F(\bar{u}_{j-p}^n, \dots, \bar{u}_{j+m}^n)$, (p and m positive*
 377 *integers) satisfies the following conditions*

- 378 1. $F(u, \dots, u) = f(u)$ (consistency)
 379 2. $F(\bar{u}_{j-p}, \dots, \bar{u}_{j+m})$ is at least Lipschitz continuous in all of its arguments.

380 *Consistency*

381 First note that the scheme is clearly built on a stencil with a finite number of
 382 cells. Let then x_{j-p}, \dots, x_{j+m} be the cell centers in the stencil containing the data
 383 needed to compute the numerical flux at the interface $x_{j+1/2}$, with p and m positive
 384 integers.

385 If $\bar{u}_{j-p}^n = \dots = \bar{u}_{j+m}^n = U$, then, since any piecewise polynomial reconstruction
 386 interpolates constants exactly, also the reconstructed point values satisfy $u_{j-p}^n = \dots =$
 387 $u_{j+m}^n = U$. Then the transformed variables are $v_{j-p}^n = \dots = v_{j+m}^n = V = \mathcal{M}^{-1}(U)$.
 388 Again, the piecewise polynomial reconstruction preserves constants, thus the num-
 389 erical derivative is zero, and all stage values in (2.14) reduce to $v_k^{(l)} = v_k^n =$
 390 $V, \forall k$ in the stencil of the cell j . Reconstructing these data, all boundary ex-
 391 trapolated data result in $v_{j+1/2}^{(l),\pm} = V$. Mapping back to conservative variables,
 392 $u_{j+1/2}^{(l),\pm} = \mathcal{M}(V) = U$. Since we are using a conservative and consistent numerical
 393 flux, $F_{j+1/2}^{(l)} = F(u_{j+1/2}^{(l),+}, u_{j+1/2}^{(l),-}) = F(U, U) = f(U)$. Finally, the numerical flux of
 394 the scheme is $F_{j+1/2} = \sum_l b_l F_{j+1/2}^{(l)} = f(U) \sum_l b_l$. So, the consistency of the numer-
 395 ical flux relies ultimately on the consistency of the RK scheme, which ensures that
 396 $\sum b_l = 1$.

397 *Lipschitz regularity*

398 All ingredients used in the construction of the numerical fluxes are at least Lip-
 399 schitz continuous. More precisely, for the second order scheme, the piecewise linear
 400 reconstruction using MinMod has just Lipschitz regularity, while WENO reconstruc-
 401 tions are C^∞ . The Lax Friedrichs numerical flux is also C^∞ . The final numerical flux
 402 is just a composition of these functions, and thus it has the required smoothness.

403 **4. Applications and numerical results.** We illustrate the performance and
 404 the field of applicability of the scheme with examples and numerical tests. We start
 405 from scalar conservation laws, where it is easy to appreciate the differences between
 406 standard conservative finite volume schemes and the new semiconservative schemes.
 407 Next we continue with classical Euler equations, to end with the equations of rela-
 408 tivistic gas dynamics, where the new scheme permits to obtain considerable savings
 409 in computational complexity.

410 **4.1. Burgers' equation.** The computation of the correct shock speeds is as-
 411 sured by the Lax Wendroff theorem, which uses only the *consistency* of the numerical
 412 fluxes, appearing in the conservative form of the finite volume formulation.

413 As an example, consider the following two initial value problems,

414 (4.1) $\partial_t u + \partial_x \left(\frac{1}{2} u^2 \right) = 0, \quad u(x, t = 0) = u_0(x) > 0$

415 (4.2) $\partial_t z + \partial_x \left(\frac{1}{3} \sqrt{(2z)^3} \right) = 0, \quad z(x, t = 0) = \frac{1}{2} u_0^2(x).$
416

417 If, in the second equation, we take the change of variables $z = \mathcal{M}(v) = \frac{1}{2} v^2$, we
418 find that in the v variables, (4.2) coincides with the characteristic form of (4.1),
419 namely $v_t + v v_x = 0$, with the same initial data. Thus the two equations have the
420 same solution, as long as the solution is smooth. However, an initial step $u_0(x) =$
421 $u_L + (u_R - u_L)H(x)$, where H is the Heavyside function, yields two different shock
422 speeds in the two initial value problems, namely

423
$$s_u = \frac{1}{2}(u_L + u_R)$$

424
$$s_z = \frac{2}{3} \frac{u_L^2 + u_L u_R + u_R^2}{u_L + u_R}$$

425

426 In fact, (4.1) prescribes the conservation of the quantity u , while the second equation
427 prescribes the conservation of the quantity z , and this fact yields two different results
428 for the shock speed, when one applies the Rankine Hugoniot condition.

429 In the standard Fully Conservative scheme, the final update and all stage values
430 are computed directly from the two conservation laws. In the Semi-Conservative
431 approach, for (4.1) we choose the auxiliary variables $v = \mathcal{M}^{-1}(u) = \mathbb{I}(u)$. Then the
432 algorithm is the following (here $\lambda = \frac{\Delta t}{\Delta x}$).

- 433 • Reconstruct the point values U_j^n from cell averages, and set $V_j^n = U_j^n$.
434 • Compute the stage values using the characteristic form $v_t + v v_x = 0$,

435
$$V_j^{(l)} = V_j^n - \Delta t \sum_{k=1}^{l-1} V_j^{(k)} D_x(V^{(k)})(x_j), \quad l = 1, \dots, \nu.$$

- 436 • Use the point values of the stages to reconstruct the boundary extrapolated
437 data, $(V_{j+1/2}^{(l)})^\pm$, and obtain $(U_{j+1/2}^{(l)})^\pm = (V_{j+1/2}^{(l)})^\pm$.
438 • Apply the conservative corrector step, evaluating the numerical flux $F^{(l)} =$
439 $F(U_{j+1/2}^{(l)+}, U_{j+1/2}^{(l)-})$, consistent with $f(u) = \frac{1}{2} u^2$, obtaining the new cell aver-
440 ages

441
$$\bar{U}_j^{n+1} = \bar{U}_j^n - \lambda \sum_{l=1}^{\nu} b_l (F_{j+1/2}^{(l)} - F_{j-1/2}^{(l)}).$$

442 For (4.2), we choose $v = \mathcal{M}^{-1}(z) = \sqrt{2z}$. Then, the semiconservative SC ap-
443 proach results in the following algorithm.

- 444 • Reconstruct the point values Z_j^n from cell averages. Set $V_j^n = \sqrt{2Z_j^n}$.
445 • Compute the stage values using the characteristic form $v_t + v v_x = 0$

446
$$V_j^{(l)} = V_j^n - \Delta t \sum_{k=1}^{l-1} V_j^{(k)} D_x(V^{(k)})(x_j), \quad l = 1, \dots, \nu.$$

- 447 • Use the point values of the stages to reconstruct the boundary extrapolated
448 data, $(V_{j+1/2}^{(l)})^\pm$, and obtain $(Z_{j+1/2}^{(l)})^\pm = \frac{1}{2} [(V_{j+1/2}^{(l)})^\pm]^2$.

449
450
451
452

- Apply the conservative corrector step, evaluating the numerical flux $F^{(l)} = F\left(Z_{j+1/2}^{(l)+}, Z_{j+1/2}^{(l)-}\right)$, consistent with $f(z) = \frac{1}{3}(2z)^{(3/2)}$, obtaining the new cell averages

$$\bar{Z}_j^{n+1} = \bar{Z}_j^n - \lambda \sum_{l=1}^{\nu} b_l (F_{j+1/2}^{(l)} - F_{j-1/2}^{(l)}).$$

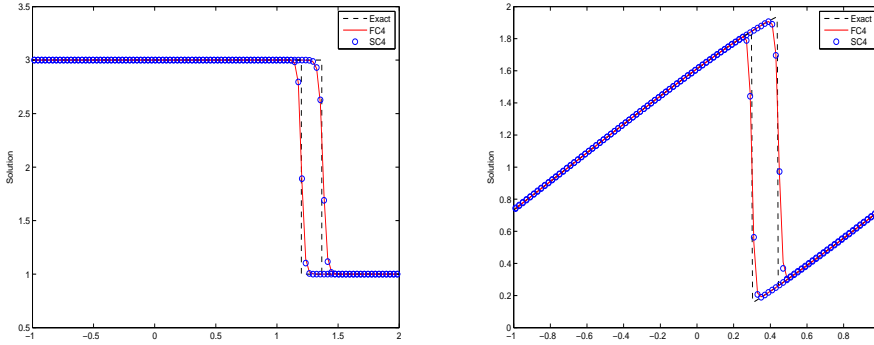


FIG. 4.1. Shock propagation (left) and shock formation (right). Red continuous line: fully conservative 4th order (FC4) scheme, blue circles: semiconservative 4th order (SC4) scheme.

453
454
455
456
457
458
459
460
461
462

The results are shown in Fig. 4.1. The plot on the left is obtained with an initial jump, located in $x = -0.8$ with $u_L = 3$ and $u_R = 1$, at time $T = 1$. The Burgers' solution is a shock travelling with speed $s_1 = 2$; the modified Burgers' (4.2) solution is a shock with speed $s_2 = \frac{13}{6}$. The plot contains the solution of both problems obtained with the fully conservative fourth order scheme (FC4) and the semiconservative fourth order scheme (SC4). The plot on the right has as initial data $u_0(x) = \sin(\pi(x - \frac{1}{2})) + 1$. For both equations the shock appears at the same time, but it will have different speeds. Note that the FC and SC solutions coincide in all cases, with the correct shock speeds. All numerical solutions were obtained with $N = 100$ grid points, and a CFL number $\text{CFL} = 0.9$.

463
464
465

4.2. Accuracy. We carry out accuracy tests on linear advection, using low and high frequency solutions, for schemes of order 2, 3 and 4. The equation is $u_t + u_x = 0$. The low frequency initial datum is

466

$$u_0(x) = \sin(\pi x - \sin(\pi x)/\pi),$$

467

while for high frequency, we consider

468

$$u_0(x) = \sin(\pi x) + \frac{1}{4} \sin(15\pi x) e^{-20x^2}.$$

469

The first test can be found in [1], while the second test is due to [29].

470

471

Figure 4.2 contains the convergence history for the low frequency (left panel) and the high frequency test (right panel). The final time is $T = 2$, with periodic boundary conditions on $[-1, 1]$, so that each solution completes a whole period. The black dashed lines are the expected rates (2, 3 and 4), the green, red and blue curves refer to the second, third and fourth order scheme respectively. The results of the fully conservative schemes are labelled with circles, while the results of the new SC

475

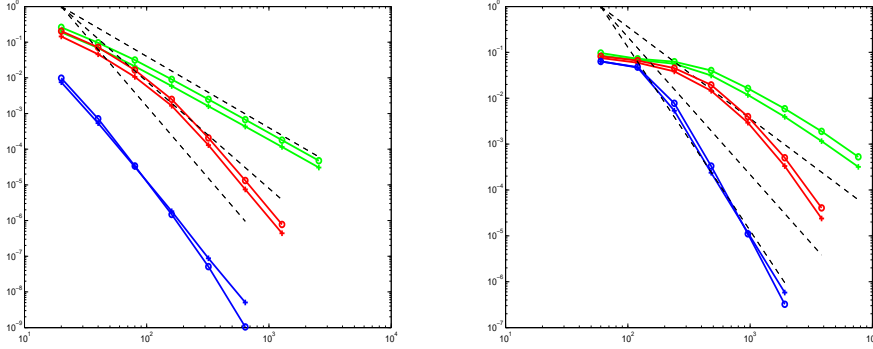


FIG. 4.2. Accuracy plots. Low frequency (left) and high frequency tests (right). From top to bottom, and green, red and blue, respectively: second, third and fourth order schemes. Semiconservative: +, and fully conservative: •.

476 schemes are marked with plus signs. The SC schemes have slightly smaller errors
 477 than the traditional FC schemes, except than in the case of the fourth order scheme.
 478 This is due to the fact that the WENO reconstruction is fifth order on the boundary
 479 extrapolated data (which are the only data needed by the fourth order FC4), but only
 480 fourth order on the reconstruction of point values at the cell center, which is needed
 481 by SC4.

482 For the data on the high frequency test, we note that the expected accuracy
 483 is obtained only after a transient, when the grid is fine enough to detect the high
 484 frequency features of the solution.

485 **4.3. Euler equations.** We consider the standard Euler equations of compressible
 486 gas dynamics in 1D. In the notation of (2.3) $U = [\rho, m, E]$, where ρ is the density,
 487 $m = \rho v$ is the momentum, v is the velocity and E is the total energy per unit volume.
 488 The pressure p is linked to the other quantities by the equation of state. Here we take
 489 $E = \frac{1}{2}\rho v^2 + \frac{1}{\gamma-1}p$, with $\gamma = 1.4$ the polytropic constant for air.

$$490 \quad (4.3) \quad \partial_t \begin{pmatrix} \rho \\ \rho v \\ E \end{pmatrix} + \partial_x \begin{pmatrix} \rho v \\ \rho v^2 + p \\ v(E + p) \end{pmatrix} = 0.$$

491 When the solution is smooth, system (4.3) can be written in terms of primitive
 492 variables, obtaining a system of the form (2.6) with $V = [\rho, v, p]$, namely

$$493 \quad (4.4) \quad \partial_t \begin{pmatrix} \rho \\ v \\ p \end{pmatrix} + \begin{pmatrix} u & \rho & 0 \\ 0 & v & 1/\rho \\ 0 & \gamma p & v \end{pmatrix} \partial_x \begin{pmatrix} \rho \\ v \\ p \end{pmatrix} = 0.$$

494 As an example, we consider Lax' Riemann Problem, which is a standard bench-
 495 mark in computational gas dynamics. The left and right states are

$$496 \quad \begin{pmatrix} \rho_L \\ v_L \\ p_L \end{pmatrix} = \begin{pmatrix} 0.445 \\ 0.6989 \\ 3.5277 \end{pmatrix} \quad \begin{pmatrix} \rho_R \\ v_R \\ p_R \end{pmatrix} = \begin{pmatrix} 0.5 \\ 0 \\ 0.5710 \end{pmatrix}$$

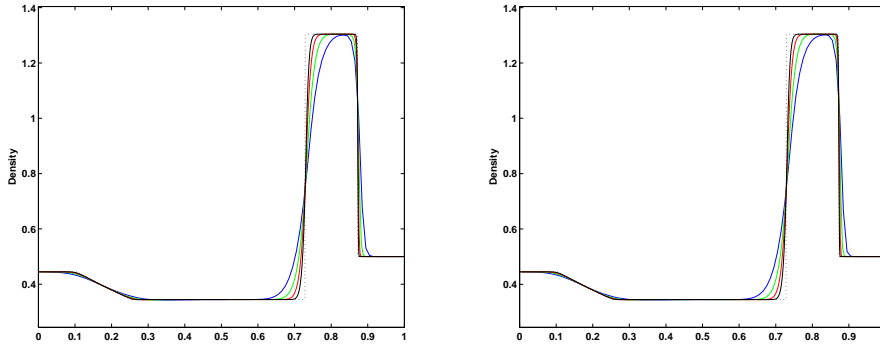


FIG. 4.3. *Lax' test, density profile with the second order FC2 (left) and SC2 (right) schemes, with $N = 100, 200, 400, 800$ (blue, green, red, black, respectively). The dashed profile is the exact solution.*

497 In this test, a high-pressure gas on the left is impinging against a stationary low
 498 pressure gas. Fig. 4.3 contains the density profiles obtained with the second order FC
 499 scheme (on the left) and the SC scheme on the right, for several values of the number
 500 of grid points: $N = 100, 200, 400, 800$. As expected, the solution converges to the
 501 exact profile (shown with the dashed line) under grid refinement, but it is noteworthy
 502 that the SC scheme and the FC one provide undistinguishable solutions.

N	FC2	SC2	FC4	SC4	FC4 CP	SC4 CP
100	0.148	0.131	0.295	0.403	9.153	9.244
200	0.213	0.224	0.745	1.002	35.44	33.42
400	0.536	0.559	2.158	2.859	143.4	130.3
800	1.493	1.557	6.940	9.037	559.6	516.4

TABLE 4.1
Computational costs for Lax' test, in seconds of CPU. The two columns on the right refer to the scheme with characteristic projection (CP)

503 We do not expect gains in efficiency in Euler equations, using the semi conservative
 504 approach, because the inverse of the map $u = \mathcal{M}(v)$, needed by the fully conservative
 505 scheme to compute the flux, can be written explicitly, and it is fast to compute. On
 506 the other hand, the SC approach requires one more reconstruction per step (from cell
 507 averages to point values), and one application of the direct map per stage, to compute
 508 the artificial diffusion correction. It is not surprising therefore that the computational
 509 times of the SC schemes are slightly higher than those obtained by the corresponding
 510 FC, see the first four columns of Table 4.1. The CPU times were obtained running
 511 the code in Matlab on a 2,9 GHz Intel Core i5 machine. The code is vectorized,
 512 except for the runs with the reconstruction on characteristic variables, as in the last
 513 two columns of the table.

514 Fig. 4.4 contains a detail of the density peak obtained with the fourth order FC4
 515 (on the left) and SC4 (on the right). It is well known that high order WENO schemes
 516 develop spurious oscillations in Riemann problems, with amplitude decreasing under
 517 grid refinement. In fact, this is precisely the meaning of *essentially* non oscillatory
 518 reconstructions. This essentially non oscillatory behaviour is quite apparent in the fig-

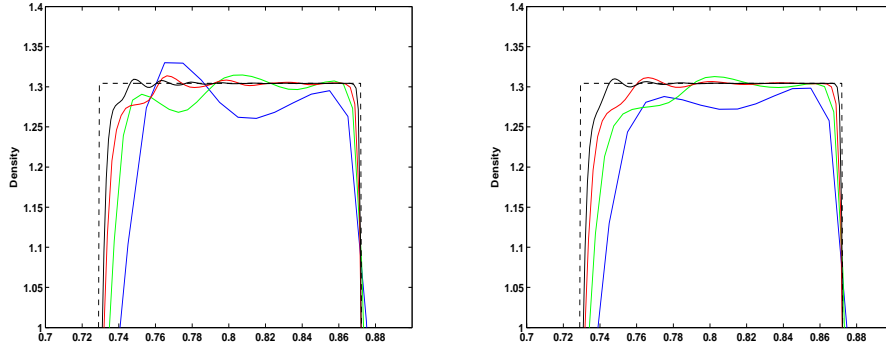


FIG. 4.4. *Lax' test, detail of the density profile with the fourth order FC_4 (left) and SC_4 (right) schemes, with $N = 100, 200, 400, 800$ (blue, green, red, black, respectively). The dashed profile is the exact solution.*

519 ure, but note that the SC solution is less oscillatory than its FC counterpart, although
 520 in both cases the amplitude of the oscillations decreases under grid refinement.

521 These oscillations arise in the first steps of the computation, when the waves
 522 originated by the Riemann problem are so close that it is impossible to find a stencil
 523 containing only one discontinuity. This problem can be cured projecting the unknown
 524 along characteristic directions, before performing the reconstruction, and computing
 525 the reconstruction along the direction of the eigenvectors. This procedure was outlined
 526 in [27] and it is very effective. The drawback is that it is computationally expensive.
 527 Fig. 4.5 shows the peak in the density of Lax' Riemann problem when this device
 528 is applied. The computational cost is reported in the last two columns of Table
 529 4.1. Now, the SC computation is slightly faster, because one variable is already a
 530 characteristic variable.

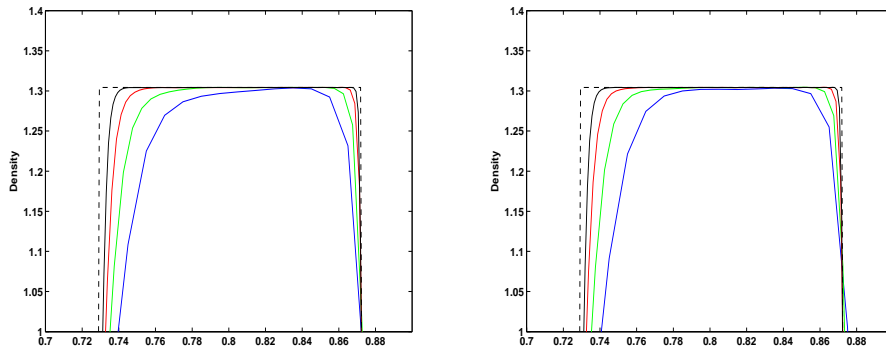


FIG. 4.5. *Lax' test, detail of the density profile with the fourth order FC_4 (left) and SC_4 (right) schemes, with $N = 100, 200, 400, 800$ (blue, green, red, black, respectively). Reconstruction along characteristic directions. The dashed profile is the exact solution.*

531 **4.4. Relativistic gas dynamics.** As we have seen in the past section, the
 532 semi-conservative approach reproduces the correct shock speeds, even though the
 533 stage values are computed in non conservative form. Since the mapping between

534 conservative and non conservative variables $u = \mathcal{M}(v)$ is easily invertible in Euler
535 equations, the semi-conservative approach is not computationally faster than standard
536 finite volume schemes. We expect to gain in efficiency when the semi-conservative
537 approach is applied to equations for which the mapping \mathcal{M} is not easily invertible.

538 As an example of this type, we consider the relativistic gas dynamic equations,
539 [22], see also [23] for a review, which can be written as

$$540 \quad (4.5) \quad \partial_t \begin{pmatrix} D \\ S \\ \tau \end{pmatrix} + \partial_x \begin{pmatrix} Dv \\ Sv + p \\ S - Dv \end{pmatrix} = 0.$$

541 where the conservative variables are mass density D , momentum density S and energy
542 density τ in the laboratory frame of reference. These quantities are linked to the
543 density ρ , the velocity v and the pressure p through the relations

$$544 \quad (4.6) \quad D = \rho W$$

$$545 \quad (4.7) \quad S = \rho h W^2 v$$

$$546 \quad (4.8) \quad \tau = \rho h W^2 - p - D,$$

548 where $W = (1 - v^2)^{-1/2}$ is the Lorentz factor in which v has been nondimensionalized
549 with the speed of light, thus $v \in [-1, 1]$; h is the enthalpy per unit mass, $h = 1 + e + \frac{p}{\rho}$,
550 and e is the internal energy per unit mass. The pressure p is given by the equation of
551 state, $p = \rho e(\gamma - 1)$. To compute the flux on the right hand side of (4.5), one must
552 compute v and p from the conservative variables.

553 The velocity v can be easily written in terms of the pressure and of conservative
554 variables using (4.7) and (4.8),

$$555 \quad v = \frac{S}{\tau + D + p}.$$

556 The internal energy is $\rho e = \rho h - \rho - p$, and the enthalpy can be written as a function
557 of the pressure and of conservative variables as

$$558 \quad \rho h = \frac{\tau + D + p}{W^2}.$$

559 Substituting these quantities in the equation of state $p = (\gamma - 1)\rho e$, one obtains a non
560 linear equation for the pressure, namely

$$561 \quad (4.9) \quad 0 = \mathfrak{F}(p(D, S, \tau)) = (\gamma W^2 - (\gamma - 1)) p - (\gamma - 1)(\tau + D(1 - W)).$$

562 The conservative variables (D, S, τ) , clearly must satisfy $D > 0, \tau > 0$. As already
563 noted, the velocity v cannot surpass the speed of light, i.e. $-1 \leq v \leq 1$. This condition
564 implies that $\tau + D \geq |S|$. Finally, the root of $\mathcal{F}(p) = 0$ must be positive, and this
565 request brings in a further restriction. In fact, $\mathcal{F}(p)$ is a monotone increasing function
566 (see [22]). Thus the pressure is positive if $\mathcal{F}(p = 0) < 0$, which is satisfied provided

$$567 \quad (4.10) \quad (\tau + D)^2 > D^2 + S^2.$$

568 In this case, the function $\mathcal{F}(p)$ has a single, positive root. To compute the flux, the
569 non linear equation (4.9) must be solved at each grid point. In our tests, (4.9) is solved
570 with Newton's method, using, as starting guess for the pressure, the local value from

571 the previous time step. Note however that condition (4.10) may be violated when
 572 spurious oscillations occur, especially when the flow is characterized by a total energy
 573 which is almost completely kinetic. In this case, (4.9) may yield a negative value
 574 for the pressure or no solution at all, and the integration breaks down. Thus, it is
 575 crucial to use non oscillatory schemes when dealing with low pressure, relativistic gas
 576 dynamics.

577 Clearly, if $v \ll 1$, classical mechanics holds, and one recovers standard compress-
 578 ible gas dynamics.

579 The equations of relativistic gas dynamics in primitive variables, are [22]

$$580 \quad (4.11) \quad \partial_t \begin{pmatrix} \rho \\ v \\ p \end{pmatrix} + \begin{pmatrix} v & \frac{\rho}{1-v^2c^2} & \frac{-v}{hW^2(1-v^2c^2)} \\ 0 & v\frac{1-c^2}{1-v^2c^2} & \frac{1}{\rho hW^4(1-v^2c^2)} \\ 0 & \frac{\rho hc^2}{1-v^2c^2} & \frac{v(1-c^2)}{1-v^2c^2} \end{pmatrix} \partial_x \begin{pmatrix} \rho \\ v \\ p \end{pmatrix} = 0,$$

581 where $c^2 = \gamma p / (\rho h)$. These are the equations which will be used in the computa-
 582 tion of the stage values.

583 Now, for the standard finite volume scheme FC, given the cell averages $\bar{D}^n, \bar{S}^n, \bar{\tau}^n$
 584 one needs to compute the ν stage values, and each stage value requires the evaluation
 585 of the inverse of the map $U = \mathcal{M}(V)$ defined by (4.6-4.8), which needs the solution
 586 of $\mathcal{F}(p; D^{(i)}, S^{(i)}, \tau^{(i)}) = 0$. In the semiconservative schemes SC, instead, given the
 587 cell averages $\bar{D}^n, \bar{S}^n, \bar{\tau}^n$, we compute the point values D^n, S^n, τ^n , and the primitive
 588 variables ρ, v, p inverting again the map $U = \mathcal{M}(V)$, but this is done only once
 589 per time step. Next, the ν stages are computed from equation (4.11), which does
 590 not require the inversion of $\mathcal{M}(V)$. Once the stage values $\rho^{(i)}, v^{(i)}, p^{(i)}$ are known,
 591 the stage values for the conservative variables $D^{(i)}, S^{(i)}, \tau^{(i)}$ are easily found. This
 592 explains why the new SC schemes are faster with respect to the fully conservative
 593 schemes in the relativistic case.

594 We illustrate the behavior of the schemes with three shock tube problems. The
 595 first two tests can be found in [22]. The left and right states for the first test are given
 596 by

$$597 \quad \text{Test 1} \quad \begin{pmatrix} \rho \\ v \\ p \end{pmatrix}_L = \begin{pmatrix} 10 \\ 0 \\ 13.3 \end{pmatrix}, \quad \begin{pmatrix} \rho \\ v \\ p \end{pmatrix}_R = \begin{pmatrix} 1 \\ 0 \\ 0.6 \cdot 10^{-6} \end{pmatrix}.$$

598 In this case, a gas expands into an extremely low pressure gas. The polytropic pa-
 599 rameter is $\gamma = \frac{5}{3}$, the final time is $T = 0.36$, and the Courant number is CFL= 0.45
 600 for all schemes. The profiles for density, velocity and pressure for the second order
 601 FC2 and SC2 can be seen in Fig. 4.6. The exact solution was computed thanks to
 602 the Riemann solver described in [23].

603 It is apparent that all features of the solution are correctly reproduced by the semi-
 604 conservative SC scheme. For the fourth order schemes, we show a peak of the density
 605 profiles in Fig. 4.7. Again, we note that the semidiscrete SC schemes are less oscilla-
 606 tory than the standard finite volume method of the same order. The computational
 607 times of the four schemes tested are listed in Table 4.2. Now, the semiconservative
 608 schemes are faster than their fully conservative counterpart, because the costly in-

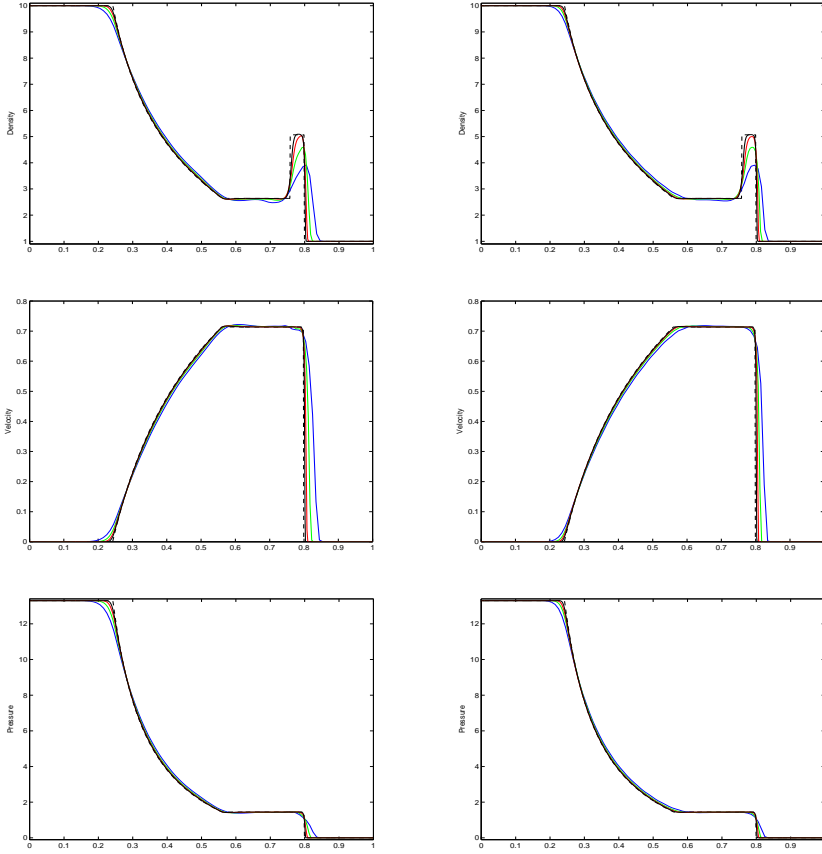


FIG. 4.6. *Martí Müller Test 1, density, velocity and pressure profiles with the second order FC2 (left) and SC2 (right) schemes, with $N = 100, 200, 400, 800$ (blue, green, red, black, respectively). The dashed profile is the exact solution.*

609 verse of the map $u = \mathcal{M}(v)$ has to be computed only once per time step. Clearly, the
 610 difference is much more apparent in the fourth order case.

N	FC2	SC2	FC4	SC4
100	0.155	0.288	0.668	0.409
200	0.341	0.260	1.390	0.788
400	0.798	0.577	3.763	1.922
800	1.973	1.506	10.783	5.611

TABLE 4.2

Computational costs for Relativistic gas dynamics, in seconds of CPU. Test 1 from Martí Müller.

611 The second test is again from [22], but an analogous set up can also be found in
 612 [26]. [33]

613 **Test 2**
$$\begin{pmatrix} \rho \\ v \\ p \end{pmatrix}_L = \begin{pmatrix} 1 \\ 0 \\ 1000 \end{pmatrix}, \quad \begin{pmatrix} \rho \\ v \\ p \end{pmatrix}_R = \begin{pmatrix} 1 \\ 0 \\ 0.01 \end{pmatrix}.$$

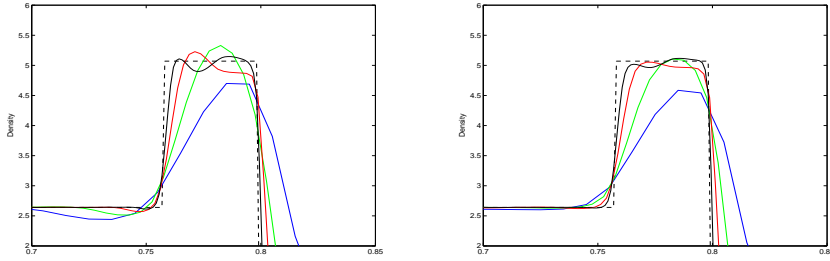


FIG. 4.7. *Martí Müller Test 1*, zoom on the density profiles with the fourth order FC_4 (left) and SC_4 (right) schemes, with $N = 100, 200, 400, 800$ (blue, green, red, black, respectively). The dashed profile is the exact solution.

614 This shock tube problem results in a rarefaction moving towards the left and a contact
 615 and shock travelling right. The difficulty of this test is due to the fact that the
 616 contact and the shock travel with almost equal speeds, so that high order schemes
 617 have difficulties in selecting a non oscillatory stencil.

618 The results obtained with the fourth order semiconservative scheme appear in Fig.
 619 4.8. The fully conservative, fourth order scheme fails on this test, because condition
 620 (4.10) is violated across the contact wave, after the computation of the first stage
 621 values.

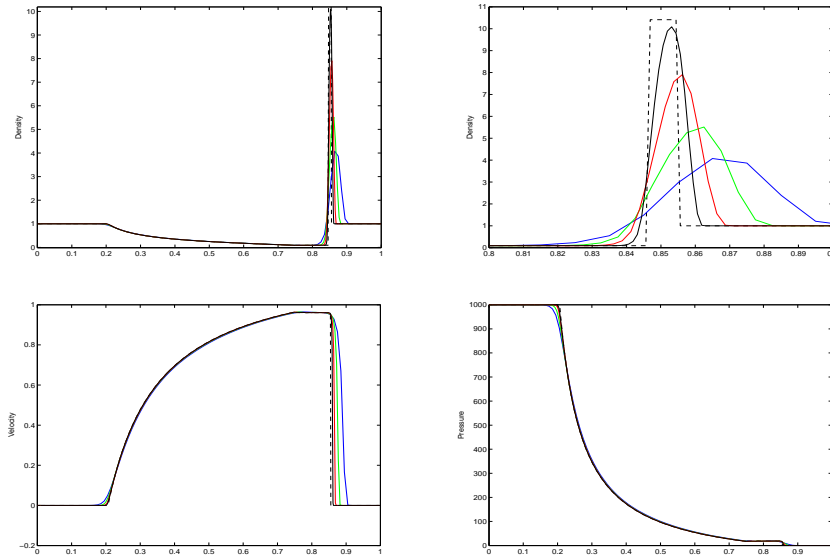


FIG. 4.8. *Martí Müller Test 2*. At the top: density profile with a zoom on the contact wave. Bottom, velocity and pressure, SC_4 with $N = 100, 200, 400, 800$ (blue, green, red, black, respectively). The dashed profile is the exact solution.

622 A further test, Test 3, is drawn from [33]. The initial left and right states are

623 given by

624 **Test 3**
$$\begin{pmatrix} \rho \\ v \\ p \end{pmatrix}_L = \begin{pmatrix} 1 \\ 0.9 \\ 1 \end{pmatrix}, \quad \begin{pmatrix} \rho \\ v \\ p \end{pmatrix}_R = \begin{pmatrix} 1 \\ 0 \\ 10 \end{pmatrix}.$$

625 It describes a low pressure gas impinging against a high pressure gas. Fig. 4.9 contains
 626 the resulting density profiles, for the fourth order schemes, with a zoom on the contact
 627 wave on the bottom of the figure. In this case, the semiconservative scheme is more
 628 oscillatory than the fully conservative finite volume scheme.

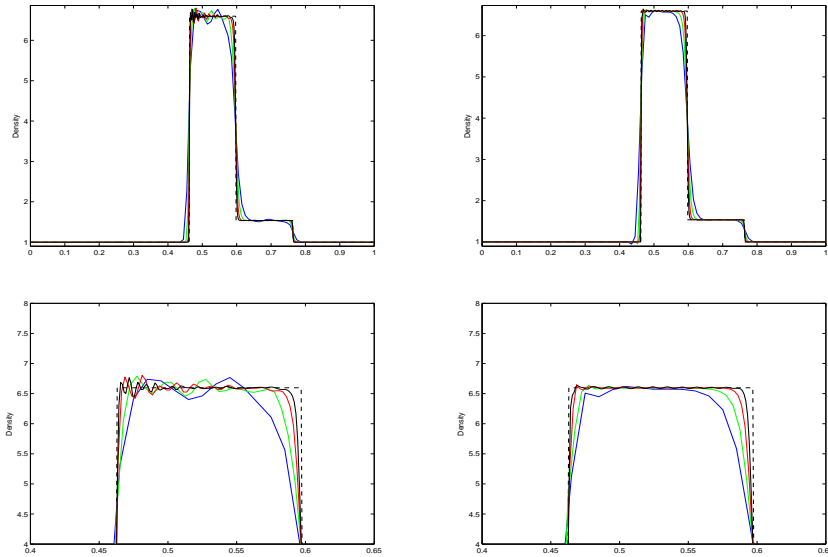


FIG. 4.9. Zhao Tang, Test 3. At the top: density profiles for SC4 (left) and FC4(right). Bottom: zoom on the contact wave. $N = 100, 200, 400, 800$ (blue, green, red, black, respectively). The dashed profile is the exact solution.

629 For this test, we also show the error versus the CPU time of first (green), second (blue)
 630 and fourth (red) order schemes. The results obtained with the fully conservative FC
 631 schemes are represented with a dot, while the results yielded by the semiconservative
 632 schemes appear with a + marker. It is clear that the SC schemes in all cases (except
 633 on a very coarse grid) yield consistently smaller CPU times for the same error. This
 634 is not a test in which high order schemes work at their best, because the solution of
 635 a Riemann problem is not full of structure. However, in this case the exact solution
 636 is known and quantitative results can be carried out. The most interesting point, is
 637 that SC is indeed faster than fully conservative schemes.

638

639 **4.4.1. Two dimensional tests.** Finally, we consider two dimensional tests.
 640 The equations for relativistic gas dynamics in primitive variables are

641

642 (4.12)
$$\partial_t V + A_x \partial_x V + A_y \partial_y V = 0,$$

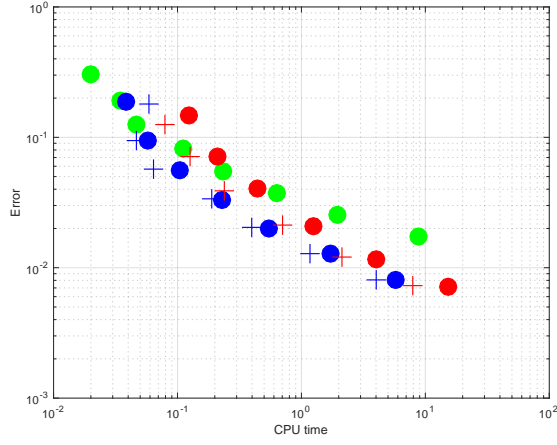


FIG. 4.10. Error versus CPU time of first (green), second (blue) and fourth (red) order schemes. FC schemes are represented with a dot, SC schemes appear with a + marker

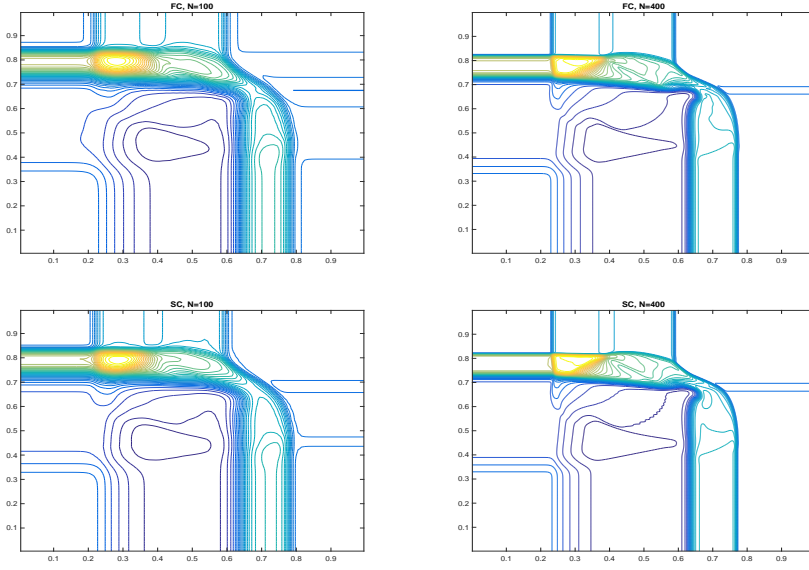


FIG. 4.11. Two-dimensional Riemann problem for relativistic gas dynamics, density contours, second order FC (top) and SC (bottom, with $N = 100$ (left), and $N = 400$ (right) points per direction.

643 where the Jacobians of the flux are given by

$$644 \quad (4.13) \quad A_x = \begin{pmatrix} u & \rho G & 0 & -\frac{uG}{hW^2} \\ 0 & uG(1-c^2) & 0 & \frac{G}{\rho hW^2}(1-u^2-c^2v^2) \\ 0 & -\frac{c^2G}{W^2}v & u & -\frac{G(1-c^2)}{\rho hW^2}uv \\ 0 & \rho hc^2G & \emptyset^2 & G(1-c^2)u \end{pmatrix}$$

645 and

$$646 \quad (4.14) \quad A_y = \begin{pmatrix} v & 0 & \rho G & -\frac{uG}{hW^2} \\ 0 & v & -\frac{c^2 G}{W^2} u & -\frac{G(1-c^2)}{\rho h W^2} uv \\ 0 & 0 & -G(1-c^2)v & \frac{G}{\rho h W^2} (1-c^2 u^2 - v^2) \\ 0 & 0 & \rho h c^2 G & G(1-c^2)v \end{pmatrix}.$$

647 Here, (u, v) are the components of the velocity in the x and y directions, respectively,
 648 $W^2 = 1/(1 - (u^2 + v^2))$ and $G = 1/(1 - c^2(u^2 + v^2))$. As a test, we propose a
 649 two-dimensional Riemann problem, in which the four states are given by

$$650 \quad V_{NW} = \begin{pmatrix} 2 \\ 0 \\ 0 \\ 1 \end{pmatrix} \quad V_{NE} = \begin{pmatrix} 2 \\ -0.5 \\ 0.5 \\ 1 \end{pmatrix} \quad V_{SW} = \begin{pmatrix} 2 \\ 0 \\ 0.5 \\ 1 \end{pmatrix} \quad V_{SE} = \begin{pmatrix} 2 \\ 0 \\ 0.5 \\ 10 \end{pmatrix},$$

651 with NW labelling the North West corner of the computational domain, and similarly
 652 for the other labels.

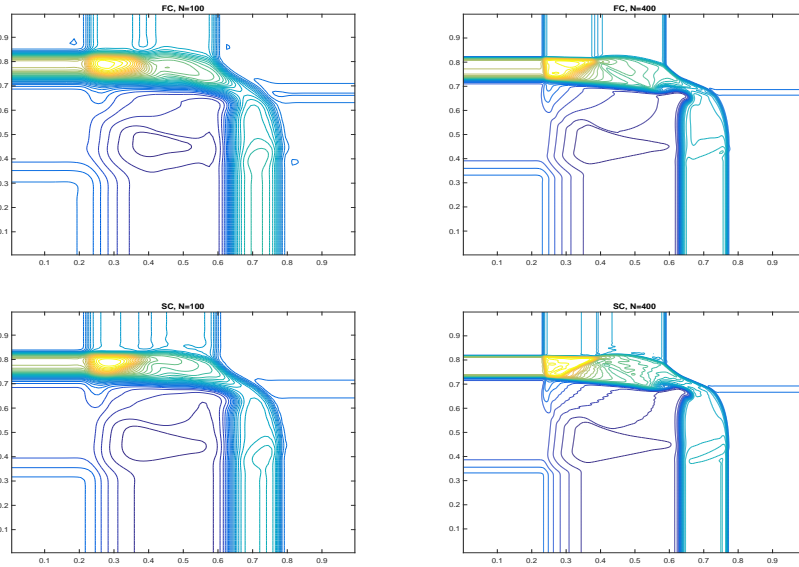


FIG. 4.12. Two-dimensional Riemann problem for relativistic gas dynamics, density contours, third order FC (top) and SC (bottom, with $N = 100$ (left), and $N = 400$ (right) points per direction.

653 The computational domain is the square $Q = (0, 1)^2$, with free-flow boundary con-
 654 ditions. The final time is $t_f = 0.36$ and the origin of the Riemann Problem is in the
 655 middle of Q .

656 We show results obtained with a dimension by dimension piecewise linear reconstruc-
 657 tion for second order, and the truly 2D third order CWENO reconstruction of [4],

658 to which we added the computation of the slopes. The results can be seen in Fig.
 659 4.11 for the second order scheme and 4.12 for the third order scheme. Each figure
 660 contains 40 contour lines for the density ρ for the FC scheme (top plots) and for the
 661 SC scheme at the bottom. The figure shows also the effect of grid refinement: the
 662 number of grid points along each side is $N = 100$ for the left plots and $N = 400$
 663 for the plots on the right. SC provides in all cases a slight improvement in the resolution
 664 of the discontinuities. Further, in this solution with a rich structure, the third order
 665 solution exhibits more details than the second order case.

666 The corresponding computational times can be found in Table 4.3. As in the 1D
 667 case, the SC scheme is faster than its corresponding FC, and the computational gain
 668 increases with the order.

N	FC2	SC2	FC3	SC3
100	1.78	1.82	12.85	9.55
200	13.45	11.54	165.25	121.19
400	138.09	113.88	1875.12	1400.89

TABLE 4.3
 Computational costs for the 2D relativistic Riemann problem, in seconds of CPU.

669 **5. Conclusions.** In this paper we have presented a novel approach to construct
 670 conservative finite volume methods for conservation laws. Although the final scheme
 671 is conservative, and is able to capture shocks with the correct propagation speed,
 672 most of the computational work is performed using a non conservative formulation,
 673 in non conservative variables. This adds a tremendous flexibility in the choice of the
 674 unknown variables and on the form of the equations on which most of the compu-
 675 tational effort is carried out. We explore in some details two applications, namely
 676 classic and relativistic gas dynamics. In both cases, the non conservative form of the
 677 equations based on primitive variables is chosen. In classical gas dynamics, it is ob-
 678 served that in many cases this choice provides much less oscillatory solutions than in
 679 standard WENO schemes based on conservative variables. In relativistic gas dynam-
 680 ics, high order schemes greatly benefit from the non-conservative formulation, which
 681 allows to compute the evolution of the fields without solving the nonlinear equation
 682 to determine the pressure from the conservative variables. Such equation has to be
 683 solved only once per cell per time step, as opposed to what happens in standard finite
 684 volume schemes based on ν stages Runge-Kutta schemes, for which such equation has
 685 to be solved ν times per cell per time step.

686 The method can be easily extended to the construction of conservative finite-
 687 difference schemes, which may be very convenient for efficient computation in several
 688 space dimensions.

689 We believe there are several other contexts in which the flexibility introduced by
 690 the semi conservative approach can be successfully exploited for producing more effec-
 691 tive codes, which are either more efficient or more accurate for the same discretization
 692 parameters. The use of the new approach in other contexts as well as in several space
 693 dimensions is currently under investigation.

694 **Acknowledgments.** The research has been partially funded by ITN-ETN Marie-
 695 Curie Horizon 2020 program ModCompShock, *Modeling and computation of shocks*
 696 *and interfaces*, Project ID: 642768; by project F.I.R. 2014 *Charge transport in graphene*
 697 *and low dimensional systems*, University of Catania; and by INDAM-GNCS 2017 re-
 698 search project *Numerical methods for hyperbolic and kinetic equation and applications*.

- 700 [1] F. ARÀNDIGA, A. BAEZA, A. M. BELDA, AND P. MULET, *Analysis of WENO schemes for full*
701 *and global accuracy*, SIAM J. Numer. Anal., 49 (2011), pp. 893–915.
- 702 [2] F. BIANCO, G. PUPPO, AND G. RUSSO, *High order central schemes for hyperbolic systems of*
703 *conservation laws*, SIAM Journal of Scientific Computing, 21 (1999), pp. 294–322.
- 704 [3] P. CARLINI, E. FERRETTI, AND G. RUSSO, *A weighted essentially nonoscillatory, large time-*
705 *step scheme for Hamilton-Jacobi equations*, SIAM Journal of Scientific Computing, 23,
706 no.3 (2005), pp. 1071–1091.
- 707 [4] M. CASTRO AND M. SEMPLICE, *Third and fourth order well-balanced schemes for the shallow*
708 *water equations based on the cweno reconstruction*, ArXiv., (2018), p. 1807.10069.
- 709 [5] M. J. CASTRO, J. M. GALLARDO, AND A. MARQUINA, *Approximate Osher-Solomon*
710 *schemes for hyperbolic systems*, Applied Mathematics and Computation, 272 (2016),
711 pp. 347 – 368, <https://doi.org/https://doi.org/10.1016/j.amc.2015.06.104>, [http://www.](http://www.sciencedirect.com/science/article/pii/S0096300315008851)
712 [sciencedirect.com/science/article/pii/S0096300315008851](http://www.sciencedirect.com/science/article/pii/S0096300315008851). Recent Advances in Numerical
713 Methods for Hyperbolic Partial Differential Equations.
- 714 [6] I. CRAVERO, G. PUPPO, M. SEMPLICE, AND G. VISCONTI, *CWENO reconstructions for balance*
715 *laws*, Math. of Comp., (2018).
- 716 [7] I. CRAVERO AND M. SEMPLICE, *On the accuracy of WENO and CWENO reconstructions of*
717 *third order on nonuniform meshes.*, J. Sci. Comput., (2016).
- 718 [8] C. DAFERMOS, *Hyperbolic Conservation Laws in Continuum Physics*, Springer, Heidelberg,
719 third ed., 2010.
- 720 [9] P. DEGOND, P.-F. PEYRARD, G. RUSSO, AND P. VILLEDIEU, *Polynomial upwind schemes for hy-*
721 *perbolic systems*, Comptes Rendus de l'Académie des Sciences - Series I - Mathematics, 328
722 (1999), pp. 479 – 483, [https://doi.org/https://doi.org/10.1016/S0764-4442\(99\)80194-3](https://doi.org/https://doi.org/10.1016/S0764-4442(99)80194-3),
723 <http://www.sciencedirect.com/science/article/pii/S0764444299801943>.
- 724 [10] E. GODLEWSKI AND P. RAVIART, *Hyperbolic systems of conservation laws*, Mathématiques &
725 *Applications, Société de Mathématiques Appliquées et Industrielles*, 1991.
- 726 [11] E. GODLEWSKI AND P. A. RAVIART, *Numerical approximation of hyperbolic systems of conser-*
727 *vation laws*, Applied Mathematical Sciences, 118, Springer-Verlag, New York, 1996.
- 728 [12] S. GOTTLIEB, C. SHU, AND E. TADMOR, *Strong stability preserving high order time discretiza-*
729 *tion methods*, SIAM Review, 43 (2001), pp. 89–112.
- 730 [13] E. HAIRER, S. P. NORSETT, AND G. WANNER, *Solving Ordinary Differential Equations I. Non-*
731 *stiff problems.*, vol. 8 of Comput. Mathematics, Springer-Verlag, 1993.
- 732 [14] E. HARABETIAN AND R. PEGO, *Nonconservative hybrid shock capturing schemes*, Journal of
733 *Computational Physics*, 105(1) (1993), pp. 1–13.
- 734 [15] G.-S. JIANG AND C.-W. SHU, *Efficient implementation of weighted eno schemes*, Journal of
735 *Computational Physics*, 126 (1996), pp. 202–228.
- 736 [16] G.-S. JIANG AND E. TADMOR, *Nonoscillatory central schemes for multidimensional hyperbolic*
737 *conservation laws*, SISC, 19 (1998), pp. 1892–1917.
- 738 [17] R. J. LE VEQUE, *Numerical Methods for Conservation Laws*, Lecture Notes in Mathematics
739 ETH Zürich, Birkhäuser Verlag, Basel, second ed., 1992.
- 740 [18] R. J. LE VEQUE, *Finite Volume methods for Hyperbolic Problems*, Cambridge University Press,
741 2002.
- 742 [19] D. LEVY, G. PUPPO, AND G. RUSSO, *Central WENO schemes for hyperbolic systems of con-*
743 *servation laws*, Mathematical Modelling and Numerical Analysis, 33 (1999), pp. 547–571.
- 744 [20] D. LEVY, G. PUPPO, AND G. RUSSO, *Compact central WENO schemes for multidimensional*
745 *conservation laws*, SIAM J. Sci. Comput., 22 (2000), pp. 656–672.
- 746 [21] D. LEVY, G. PUPPO, AND G. RUSSO, *A fourth-order central WENO schemes for multidimen-*
747 *sional hyperbolic systems of conservation laws*, SIAM Journal of Scientific Computing, 24
748 (2002), pp. 480–506.
- 749 [22] J. MARTÌ AND E. MÜLLER, *Extension of the piecewise parabolic method to one-dimensional*
750 *relativistic hydrodynamics*, Journal of Computational Physics, 123 (1996), pp. 1–14.
- 751 [23] J. MARTÌ AND E. MÜLLER, *Numerical Hydrodynamics in Special Relativity*, Living Reviews in
752 *Relativity*, Max Planck Institute, 2003.
- 753 [24] H. NESSYAHU AND E. TADMOR, *Non-oscillatory central differencing for hyperbolic conservation*
754 *laws*, Journal of Computational Physics, 87 (1990), pp. 408–463.
- 755 [25] L. PARESCHI, G. PUPPO, AND G. RUSSO, *Central Runge-Kutta schemes for conservation laws*,
756 *SIAM Journal of Scientific Computing*, 26 (2005), pp. 979–999.
- 757 [26] S. QAMAR AND M. YOUSAF, *Application of a discontinuous Galerkin finite element method to*
758 *special relativistic hydrodynamic models*, Computers and Mathematics with Applications,
759 65 (2013), pp. 1220–1232.

- 760 [27] J. QIU AND C. SHU, *On the construction, comparison, and local characteristic decomposition*
761 *for high-order central WENO schemes*, J. Comput. Phys., 183 (2002), pp. 187–209.
- 762 [28] P. L. ROE, *Approximate riemann solvers, parameter vectors and difference schemes*, JCP, 43
763 (1981), pp. 357–372.
- 764 [29] M. SEMPLICE, A. COCO, AND G. RUSSO, *Adaptive mesh refinement for hyperbolic systems based*
765 *on third-order compact WENO reconstruction*, J. Sci. Comput., 66 (2016), pp. 692–724.
- 766 [30] J. SHI, C. HU, AND C.-W. SHU, *A technique of treating negative weights in WENO schemes*,
767 J. Comput. Phys., 175 (2002), pp. 108–127.
- 768 [31] C.-W. SHU, *Essentially Non-Oscillatory and Weighted Essentially Non-Oscillatory Schemes*
769 *for Hyperbolic Conservation Laws*, Lecture Notes in Mathematics, 1697, Springer, Berlin,
770 1998.
- 771 [32] C.-W. SHU AND S. OSHER, *Efficient implementation of essentially non-oscillatory shock-*
772 *capturing schemes*, Journal of Computational Physics, 77 (1988), pp. 438–471.
- 773 [33] J. ZHAO AND H. TANG, *Central Runge-Kutta discontinuous Galerkin methods for the special*
774 *relativistic hydrodynamics*, ArXiv, (2016), p. 1609.06792v1.